Petroleum Science 19 (2022) 3149–3158

Contents lists available at ScienceDirect

Petroleum Science

journal homepage: www.keaipublishing.com/en/journals/petroleum-science

Original Paper

High-strength and self-degradable sodium alginate/polyacrylamide preformed particle gels for conformance control to enhance oil recovery

Xiao Zhang [a, *, 1], Jia-Nan Deng [a, 1], Kai Yang [a], Qian Li [a], Sen-Yao Meng [a], Xiu-Xia Sun [a], Zhao-Zheng Song [a], Yong-Dong Tian [b], Sui-An Zhang [a, c], Xin-Jia Liu [d], Zhan-Yi Wang [a], Xin-Yu Liu [a], Gui-Wu Lu [a, **], Zi-Long Liu [a, ***]

[a] Coalbed Methane Research Center, Beijing Key Laboratory of Optical Detection Technology for Oil and Gas, College of Science, China University of Petroleum-Beijing, Beijing, 102249, China
[b] Shanxi Lanyan Coalbed Methane Group Co., Ltd, Jincheng, Shanxi, 048012, China
[c] State Key Laboratory of Coal and CBM Co-Mining in Nancun Town, Jincheng, Shanxi, 048012, China
[d] Institute of Oil and Gas Technology Research, Changqing Oilfield, CNPC, Xi'an, Shaanxi, 710021, China

ARTICLE INFO

Article history:
Received 9 February 2022
Received in revised form
6 April 2022
Accepted 16 June 2022
Available online 20 June 2022

Edited by Jia-Jia Fei

Keywords:
Conformance control
Sodium alginate
Dual cross-linked
Temporary plugging agent
High-strength
Self-degradation

ABSTRACT

Excess water production has become an important issue in the oil and gas extraction process. Preformed particle gels (PPGs), show the capability to control the conformance and reduce excess water cut. However, conventional PPGs have poor mechanical properties and their swollen particles are easily damaged by shearing force when passing through the fractures in formations, meanwhile PPGs can be also degraded into various byproducts, leading to permanent damage to the reservoir permeability after temporary plugging. Herein, a novel type of dual cross-linked PPGs (d_PPGs) was designed and synthesized using sodium alginate (SA) and acrylamide (AAm), cross-linked with N, N′-methylenebisacrylamide (MBA) and Fe^{3+}. Results show that d_PPGs have excellent mechanical properties with a storage modulus up to 86,445 Pa, which is almost 20 times higher than other reported PPGs. Meanwhile, d_PPGs can be completely degraded into liquid without any solid residues or byproducts and the viscosity of d_PPGs degraded liquid was found to be lower than 5 mPa·s. A laboratory coreflooding test showed that the plugging efficiency of d_PPGs was up to 99.83% on open fractures. The obtained results demonstrated that d_PPGs could be used as economical and environment-friendly temporary plugging agent with high-strength, self-degradation, thermal stability, and salt stability, thus making it applicable to a wide range of conformance control to enhance oil recovery.

1. Introduction

The continuous exploitation of oil and natural gas resources has led to an extremely high water cut in oil wells, and the remaining oil is mainly concentrated in low permeability reservoir matrix that cannot be swept effectively by displacement fluid. The main reason is the heterogeneity caused by fractures or highly permeable areas in the formation (Li et al., 2007, 2019; Fatemi and Kharrat, 2011; Elsharafi and Bai, 2016; Wu et al., 2019; Liu et al., 2021). A large amount of displacement fluid flows along these highly permeable areas and bypasses the oil in the low permeability areas when there are high-conductivity fractures within the formation, resulting in excessive water production and ineffective circulation of the displacement fluid (Imqam and Bai, 2015; Seright and Brattekas, 2021). Excessive water production can cause problems such as increase oil-water separation costs, operational costs, and equipment corrosion (Elsharafi and Bai, 2012; Zhao et al., 2015; Alfarge et al., 2017). For an efficient oil recovery and displacement fluid utilization, the displacement fluid needs to be diverted into the low

* Corresponding author.
** Corresponding author.
*** Corresponding author.
E-mail addresses: zhangxiao@cup.edu.cn (X. Zhang), lugw@cup.edu.cn (G.-W. Lu), zlliu89@gmail.com (Z.-L. Liu).
[1] These authors contributed equally as the first author.

https://doi.org/10.1016/j.petsci.2022.06.012

Abbreviations

AAm	Acrylamide
d_PPGs	Dual cross-linked preformed particle gels
DW	Distilled water
ESR	Equilibrium swelling ratio
FW	Formation water
HPAM	Hydrolysed polyacrylamide
MBA	N,N′-methylenebisacrylamide
PPGs	Preformed particle gels
SA	Sodium alginate
SEM	Scanning electron microscopy
TDS	Total dissolved salinity

permeability, unswept, and oil-rich areas by blocking some highly permeable areas, making the displacement process economical.

Gel treatments have been proven to be a cost-effective strategy for conformance control in the heterogeneous reservoirs (Al-Muntasheri et al., 2007; Bai et al., 2007; Kang et al., 2015; Sun and Bai, 2017). This can control the excess water production, and increase the swept areas and utilization ratio of the displacement fluid. Two dominant types of gel treatment are in situ cross-linked polymer gels and PPGs.

In situ cross-linked polymer gels form a 3D gel network to block the fractures or highly permeable areas, thus diverting the displacement fluid. This is done by pumping a polymer solution (gelling solution) and a cross-linking agent solution (gellant solution) into target zones, respectively, which react after a suitable time depending on the reservoir conditions (Ganguly et al., 2001). Partially hydrolysed polyacrylamide (HPAM) and multivalent cations systems (e.g., Cr^{3+}, Zr^{4+}, and Cr^{6+}) are commonly used and developed to be applied to formations with a highly permeable matrix, to improve their profile performance (Singh and Mahto, 2017). In situ cross-linked gels have poor gel strength; they are not environment-friendly owing to the use of toxic metal ions and have an uncertainty in gelation time that is easily affected by the formation conditions (Zhu et al., 2017).

PPGs have several extensive applications because they are synthesized to form a cross-linked polymer 3D gel network in the surface facilities, then being injected to partially or completely block high-permeability areas, diverting the displacement fluid to low-permeability areas (Khoshkar et al., 2020). PPGs can be produced in different size scales (from micrometres to centimetres), depending on the application, by drying, crushing, and screening the preformed gels (Imqam and Bai, 2015). Hydrophilic functional groups in PPGs structures, such as carboxyl groups (−COOH), hydroxyl groups (−OH), and amide groups ($-CONH_2$), cause them to swell in aqueous solutions, thus making them elastic and deformable. This allows them to plug fractures and highly permeable areas in the formation, to control the water flow (Bai et al., 2007). PPGs can overcome some of the drawbacks of in situ cross-linked polymer gels and have a relatively wide range of applications because the gel formation process of PPGs is completed in the surface facilities (Liu et al., 2010; Qiu et al., 2017; Chen et al., 2021).

However, PPGs still exist some non-negligible issues that we should take into consideration. On one hand, owing to weak mechanical properties, the swollen PPGs are easily damaged by the shearing force when they pass through the fractures in the formation. On the other hand, many PPGs can cause a permanent damage to the reservoir permeability after temporary plugging because they convert to aldehydes, ketones, carboxylic groups, and some monomer units that adsorb on the surface of formation minerals (Touzé et al., 2015; Zhao et al., 2020; Masulli et al., 2021). Baloochestanzadeh et al. created a nanocomposite preformed particle gels with an enhanced elastic modulus based on starch-graft-polyacrylamide loaded with nanosilica, but the enhanced gel elastic modulus can only reach 900 Pa (Baloochestanzadeh et al., 2021). Salunkhe et al. developed ultra-high temperature resistant PPGs, stable for more than 12 months at 150 °C with an elastic modulus of 3,100 Pa, but their self-degradability was not reported (Salunkhe et al., 2021). Tongwa et al. designed self-degradable PPGs. The maximum improvement in the elastic modulus of PPGs had reached 4,100 Pa, by adding 3% nanomaterials, which is still unsatisfactory (Tongwa and Bai, 2014). As far as we know, preformed particle gels, which have both high mechanical properties and self-degradability, are still rarely studied (Zhu et al., 2020). Therefore, this study aims to design self-degradable PPGs with excellent mechanical properties and can meet the requirements of high-temperature and high-salinity oil reservoirs.

To aid biodegradability and mechanical properties of PPGs, the natural linear polymer extracted from brown algae, SA, was chosen for this experiment. It is composed of a α-L-guluronic acid (G unit) and a β-D-mannuronic acid (M unit) linked via a glycosidic bond. The SA has randomly arranged polyguluronic acid fragments (GG), polymannuronic acid fragments, and mannuronic–guluronic acid combined sections (Baumberger and Ronsin, 2010; Patel et al., 2017). The GG segments of the SA chains can chelate with metal ions (e.g., Ca^{2+}, Mg^{2+}, Al^{3+}, Cr^{3+}, and Fe^{3+}) to form an "eggshell" 3D network structure (Zheng et al., 2016; Zhou et al., 2018; Pu et al., 2021), with the ion radius and charge of cations affecting the strength of chelation (Sun et al., 2012; Yang et al., 2013; Li et al., 2014; Liu et al., 2019). This characteristic allows for a design of a hydrogel with physical cross-linking points, by introducing metal ions into the structure of SA. Furthermore, MBA can act as chemical cross-linking points through copolymerization with acrylamide, and finally construct dual cross-linked structure.

In this study, we prepared preformed particle gels with a dual cross-linked structure, by introducing natural polymer SA into the polyacrylamide network, then cross-linked with $Fe(NO_3)_3 \cdot 9H_2O$. The FTIR, SEM, swelling kinetics behavior, gel strength and stability, plugging performance, and core damage experiments of the prepared PPGs were charactered and analysed.

2. Materials and methods

2.1. Materials

Acrylamide, ammonium persulfate (APS), MBA, iron (III) nitrate nonahydrate ($Fe(NO_3)_3 \cdot 9H_2O$) were supplied by Shanghai Aladdin Biochemical Technology Co., Ltd. SA (viscosity 80–120 mPa·s) was supplied by Beijing InnoChem Science & Technology Co., Ltd.

2.2. Preparation of d_PPGs

A two-step method was used to prepare dual cross-linked PPGs by the free radical polymerization mechanism. Firstly, 0.3 g of SA, 1.68 g of AAm, and 0.0084 g of MBA (0.5 wt% relative to monomer) were dissolved in 8 g of distilled water and stirred overnight using a magnetic stirrer to ensure thorough mixing. Nitrogen gas was introduced for 30 min to remove oxygen. Then, 0.0168 g of APS (1 wt% relative to monomer) was added slowly before transferring the mixture to a 65 °C vacuum oven for 3 h, to obtain a single cross-linked hydrogel (s_hydrogel). The s_hydrogel was immersed in 2 mol/L $Fe(NO_3)_3 \cdot 9H_2O$ solution for 24 h to produce the dual cross-linked hydrogel (d_hydrogel), before transferring it into distilled

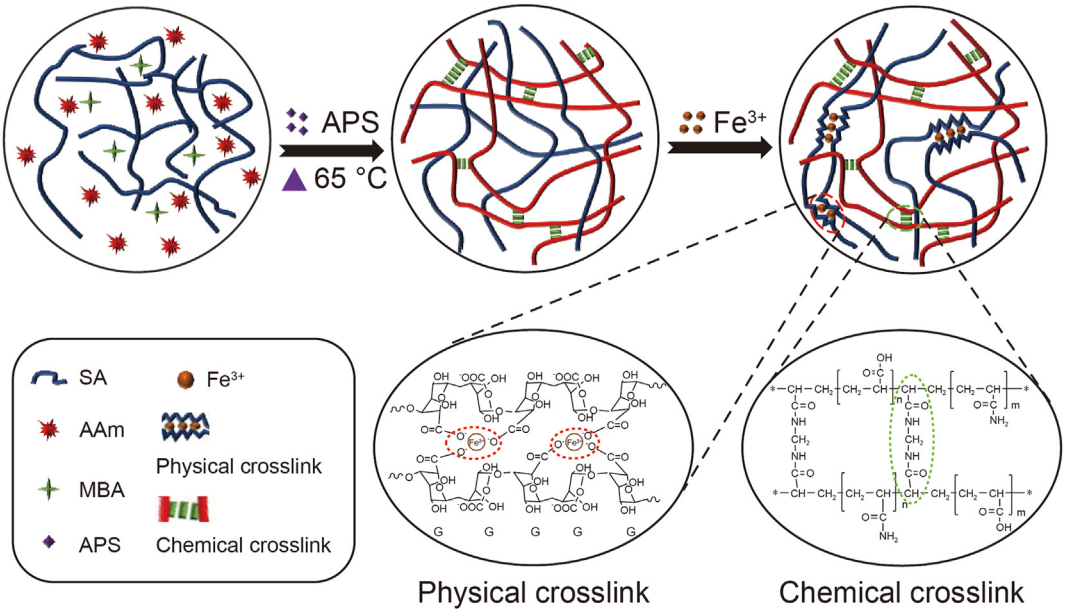

Fig. 1. Preparation of dual-crosslink (chemically and physically) preformed particle gels.

water for three days to wash away the residual Fe^{3+} (Lin et al., 2015). The prepared d_hydrogel was dried, crushed, and screened to obtain dual cross-linked preformed particle gels (d_PPGs) of a certain size. A schematic of the preparation process of d_hydrogel is shown in Fig. 1.

2.3. Characterization of d_PPGs

2.3.1. Fourier-transform infrared (FTIR) spectroscopy

Fourier-transform infrared (FTIR) spectra were obtained on a Bruker EQUINOX55 FTIR spectrophotometer to monitor the functional group changes before and after polymerization. The sample to be tested is completely dried in an oven at 60 °C until its mass remains constant, then the dried samples were ground and pelletized using KBr (1:100 w/w) for the FTIR measurements. The spectra were recorded over a frequency range of 4,000–400 cm^{-1}.

2.3.2. Scanning electron microscopy (SEM)

The micromorphology of the gels was observed at a range of magnifications using a ZEISS Gemini SEM 300 at 20 kV. The swollen hydrogel was frozen at −50 °C and then evacuated, to obtain aerogel samples. The sample was broken in liquid nitrogen to obtain a fresh fractured section, following which it was adhered to conductive glue and was sprayed with gold.

2.3.3. Swelling kinetics behavior of d_PPGs

The swelling kinetics behavior of each sample was measured at room temperature (25 °C) in distilled water. The gel sample was thoroughly dried before the measurement and then crushed and screened for 50–60 mesh, followed by immersion in distilled water until completely swollen. The swelling ratio was obtained by the following equation:

$$SR = (M_t - M_0)/M_0 \times 100$$

SR is the swelling ratio at time *t*, M_t is the mass of the dried sample after it was allowed to swell in distilled water at time *t*, and M_0 is the initial mass of the dried sample.

2.3.4. Gel strength test

The mechanical properties of d_PPGs were measured using HAAKE MARS III from Thermo Scientific. The sensor used for all measurements was a PP35 with a gap of 2 mm. The gel samples were cut in uniform dimensions with diameter of 35 mm and thickness of 2 mm. At room temperature, the storage modulus, G', and loss modulus, G'', were measured as a function of strain amplitude in the range of 0.01%–100% at a fixed frequency of 1 Hz. Data was obtained in the linear viscoelastic region wherein G' and G'' were independent of the strain amplitude. All subsequent oscillation time-dependent experiments were performed at a fixed strain amplitude of 0.5%, to obtain the values of G' and G'' as a function of frequency.

2.3.5. Gel stability test

The swelling kinetics behavior and self-degradation behavior of d_PPGs were used to evaluate the stability of their performance under different conditions (e.g., formation temperature and salinity). The test method is shown in Fig. 2. Briefly, 2 g of dried d_PPGs and 20 mL of salt solution were transferred to a hydrothermal reactor placed in a vacuum oven and aged at different set temperatures. The self-degradation time of d_PPGs is defined as the time taken for the material to change from the initial solid-state to completely transform into its liquid-state.

2.3.6. Laboratory coreflooding test

The laboratory coreflooding test was used to evaluate the plugging effect of d_PPGs on open fractures in the formation. A core of 5 cm length (L) and 2.5 cm diameter (D) was created using a copper sheet (0.8 mm thickness) in a core that was split by a Brazilian splitting test device, to imitate the fracture in the formation. A schematic of the laboratory coreflooding test is shown in Fig. 3 and was conducted in the following steps:

(1) The core was dried at 70 °C for 48 h until its weight remained constant.
(2) A vacuum pressure saturation device was used to saturate the core with formation water and the weight was measured, to calculate the pore volume and porosity.

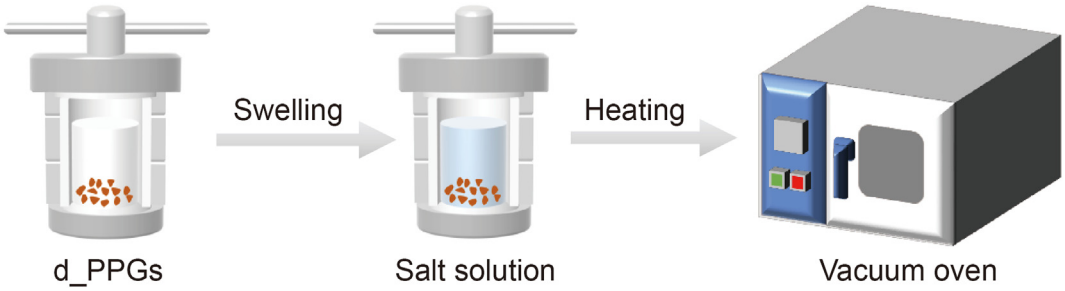

Fig. 2. Schematic diagram of d_PPGs stability test.

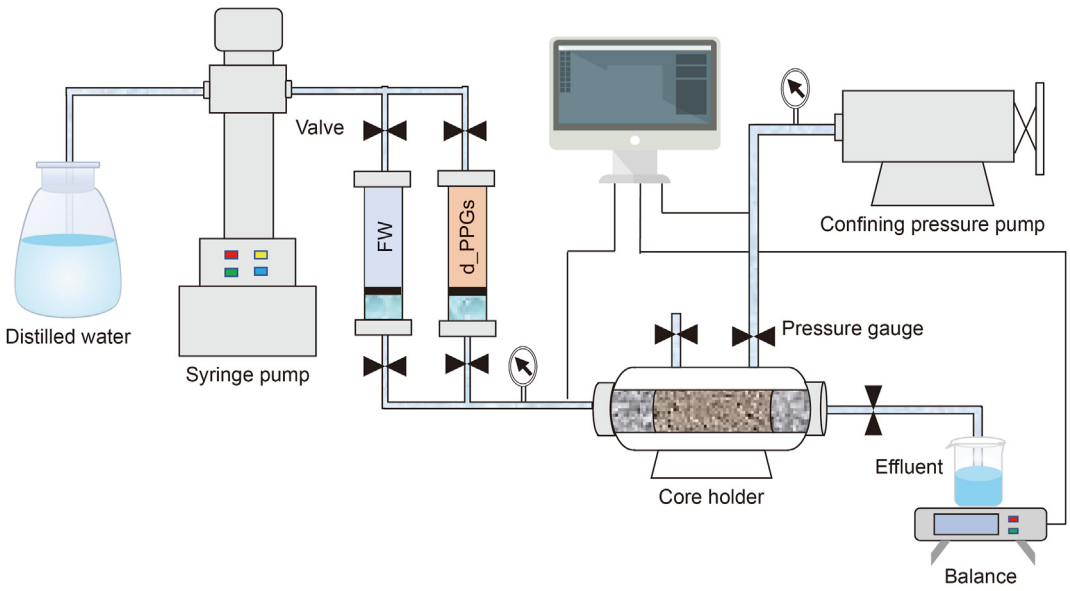

Fig. 3. Schematic of laboratory coreflooding test.

(3) The core was placed in the core holder with a confining pressure 2 MPa higher than the injection pressure.
(4) Formation water was injected at a rate of 0.5 mL/min until the flow rate and pressure difference were stabilized. The initial permeability, K_b, of the fractured core was calculated using Darcy's law.
(5) Herein, 0.5 wt% of the swollen d_PPGs solution (carried by a guar gum solution) was injected at an injection rate of 0.5 mL/min. The process was stopped when d_PPGs flowed through the outlet and the injection pressure were stable.
(6) The formation water was injected again at a rate of 0.5 mL/min, and the injection was stopped after the flow rate and pressure difference were stabilized. The permeability, K_a, of the core after plugging was calculated. The maximum pressure of the process was recorded as the breakthrough pressure. The plugging efficiency (E) is obtained by the following formula.

$$E = (K_b - K_a)/K_b \times 100$$

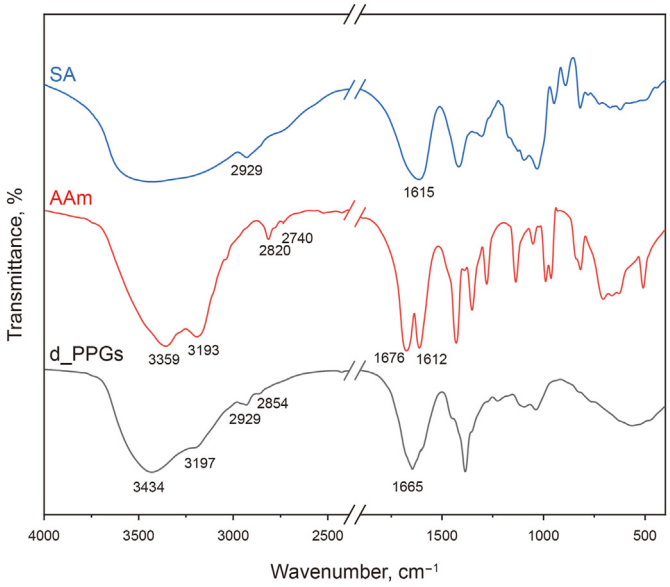

Fig. 4. Fourier-transform infrared spectrum of SA, AAm, and d_PPGs.

2.3.7. Core damage experiment

The device shown in Fig. 3 is used to conduct a core damage experiment to evaluate the effect of the degraded liquid of d_PPGs on the permeability of core matrix. The core used was unsplit sandstone. First, the first water flooding process was carried out on the sandstone core, and the permeability before damage, K_b, was calculated after the pressure difference and outlet flow rate were stabilized. Then, the degraded liquid of d_PPGs was injected in the reverse direction, and the process was stopped after the pressure difference and outlet flow rate were stabilized. The second water flooding was then performed to obtain the permeability, K_a, after the damage. The specific parameters of the experiment were found to be consistent with the laboratory coreflooding test. The core damage ratio is obtained by the following formula:

$$D = (K_b - K_a)/K_b \times 100$$

3. Results and discussion

3.1. Structural characterization by FTIR

Fig. 4 shows the FTIR spectra of SA, AAm, and d_PPGs. The SA spectrum displays a broad absorption peak around 3400 cm^{-1} due to −OH stretching vibration characteristic absorption. The characteristic peaks at 2929 cm^{-1} and 1615 cm^{-1} are due to $-CH_2$ stretching and C=O stretching, respectively. For the AAm, the absorption peaks at 3359 cm^{-1}, 3193 cm^{-1}, 2820 cm^{-1}, and 2740 cm^{-1} are due to N−H stretching vibration, =CH stretching, and $-CH_2$ stretching, respectively. The peaks at 1676 cm^{-1} and 1612 cm^{-1} were assigned to the stretching vibrations of C=O and C=C. The d_PPGs products have a broad peak between 3100 cm^{-1} and 3500 cm^{-1} owing to the superposition of the −OH and N−H absorption peaks of SA and AAm, respectively. The C=C absorption peak (around 1615 cm^{-1}) in the d_PPGs disappeared while the C=O (1665 cm^{-1}) was retained, indicating that the monomer was successfully polymerized, i.e. a complete reaction occurred.

3.2. Micromorphology of d_PPGs

The SEM images presented in Fig. 5 show that the freeze-dried d_PPGs sample have a basic hydrogel morphological structure with a honeycomb-like grid structure. These structures could greatly increase the specific surface area of the d_PPGs, improving the water absorption and water retention performance. The relatively tight network structure is due to the existence of two cross-linking points in the d_PPGs: chemical cross-linking point and physical cross-linking point. This could lead to a tighter structure during application and could improve the strength of the network after the swelling, enhancing the plugging effect.

The mapping of Fe illustrates that it is evenly distributed throughout the sample system, meaning that the prepared d_PPGs have a very uniform cross-linked structure, which will help avoid stress concentration caused by local structural defects.

3.3. Swelling kinetics behavior of d_PPGs

The swelling kinetics behavior of d_PPGs has great influence on its plugging and profile control performance. Fig. 6 shows the morphological changes of d_PPGs before and after swelling in distilled water at room temperature, illustrating that the swollen particles could still maintain their integrity. The swelling ratio of the d_PPGs increases with water absorption time before reaching the equilibrium swelling ratio (ESR). At the same time, it was found that the ESR of d_PPGs at room temperature is about 390%, and the time to reach ESR is about 400 min (Fig. 7), which ensures good transport capacity and high plugging strength (Song et al., 2019).

3.4. Gel strength test

The mechanical property of the d_PPGs sample is reflected by their storage modulus (G') and loss modulus (G''). The linear viscoelastic region is shown as the region where G' and G'' are

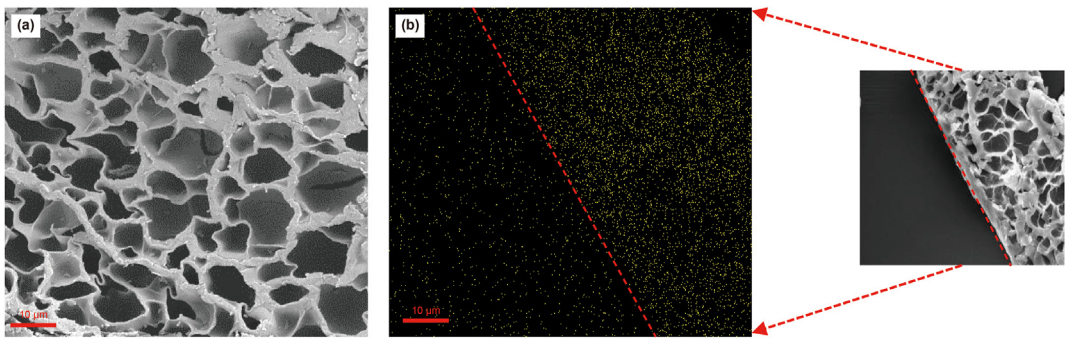

Fig. 5. **(a)** The SEM images of micromorphology of d_PPGs. **(b)** Elemental mapping of Fe in the d_PPGs.

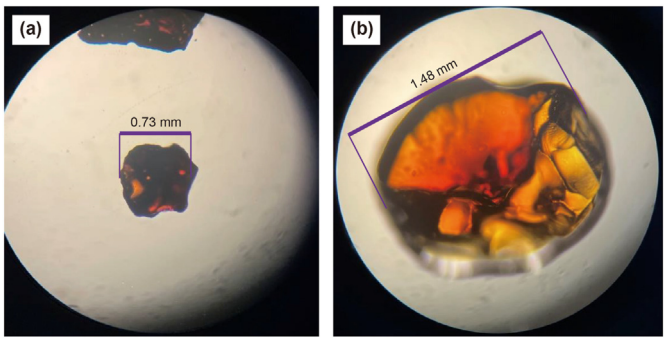

Fig. 6. The morphological changes of d_PPGs before **(a)** and after **(b)** swelling in distilled water at room temperature (25 °C).

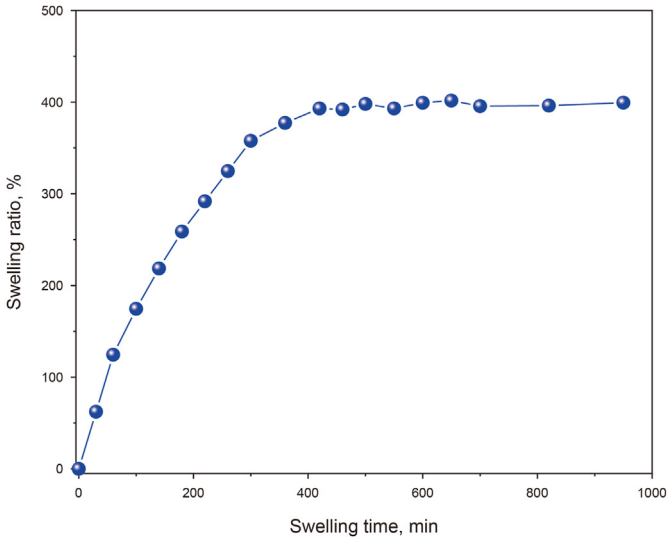

Fig. 7. Swelling kinetics behavior of d_PPGs in distilled water at room temperature (25 °C).

constant when the strain is less than 1% at a frequency of 1 Hz in Fig. 8 (a). In this region, the value of G' is always greater than the value of G'', suggesting that the 3D network structure reacts primarily elastically to low strains (Ye et al., 2014; Bao et al., 2018). Using a constant strain amplitude of 0.5%, a sweep of frequency (from 0.1 Hz to 100 Hz) shows an increase in moduli in proportion with frequency (Fig. 8 (b)). The elastic modulus of d_PPGs sample reached a maximum of 86,445 Pa, which is almost 20 times higher than other reported PPGs (Tongwa and Bai, 2014; Amaral et al., 2019). The high elastic modulus is attributed to the dual-crosslinking structure of the d_PPGs, both physical crosslinking (chelation of Fe^{3+} and COO^{-}) and chemical crosslinking (chemical linkage of MBA and AM). In addition, Fe^{3+} as the cross-linking cation can form a tighter physical cross-linking point with COO^{-}, because Fe^{3+} has larger ionic radius and higher number of charges compared with other cations. A high elastic modulus means that the gel could withstand higher stress during injection or migration. Moreover, d_PPGs with high elastic modulus also meant they could return to their original shape when the external force is removed, providing better plugging performance. As the ionic crosslinking between SA and Fe^{3+} is reversible when the external force is removed, the crosslinking could be restored, further enhancing the sample deformation ability.

3.5. Gel stability test

3.5.1. Effect of temperature on gel swelling kinetics behavior and self-degradation time

The effect of temperature on d_PPGs swelling kinetics behavior was studied using 2 g of dried d_PPGs in 20 mL of 50,000 ppm NaCl solution added to a hydrothermal reaction kettle, and then placed in a vacuum oven at different temperatures (25 °C, 50 °C, 80 °C, 100 °C, and 120 °C). The mass of the swollen d_PPGs is measured at regular intervals until it becomes constant, as shown in Fig. 9. The swelling ratio of d_PPGs initially increased rapidly and then reached the ESR, following which it remained almost constant. At higher the temperature, the ESR of d_PPGs was greater and was attained more quickly. The reason is that at higher temperatures, the chelation between Fe^{3+} and COO^{-} in d_PPGs structure will be damaged to a certain extent, thus reducing the crosslinking density of the system, and resulting in a greater ESR. The higher diffusion rate of ions at the higher temperatures lessens the time taken by the d_PPGs to attain ESR.

The swelling temperature and swelling time are further increased to evaluate the self-degradation performance of the d_PPGs, as shown in Fig. 10. This shows that as the temperature increased, the degradation time of d_PPGs decreased with significant reduction, when the temperature exceeded 80 °C. This effect can be explained by the following analysis, higher temperature endows the molecules with faster thermal motion, and at the same

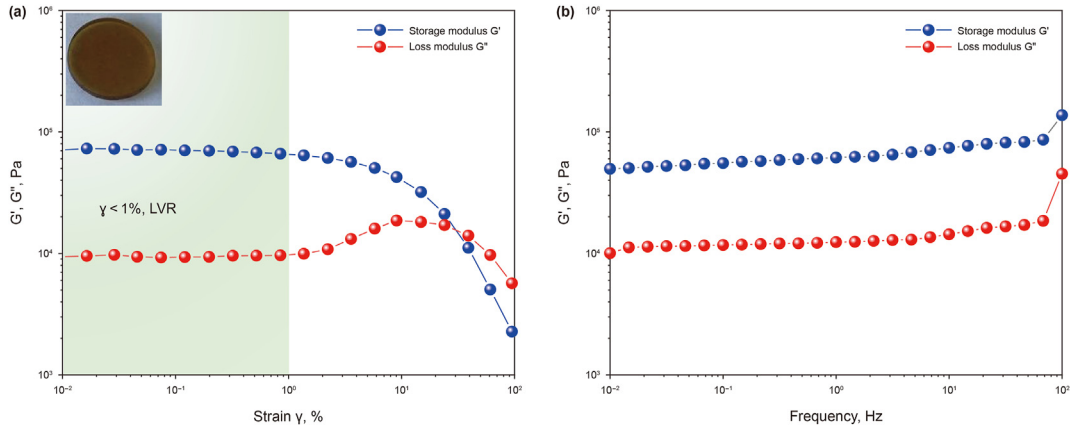

Fig. 8. The mechanical property of the d_PPGs sample. **(a)** Strain amplitude sweep from 0.01% to 100%. **(b)** Frequency sweep from 0.1 Hz to 100 Hz.

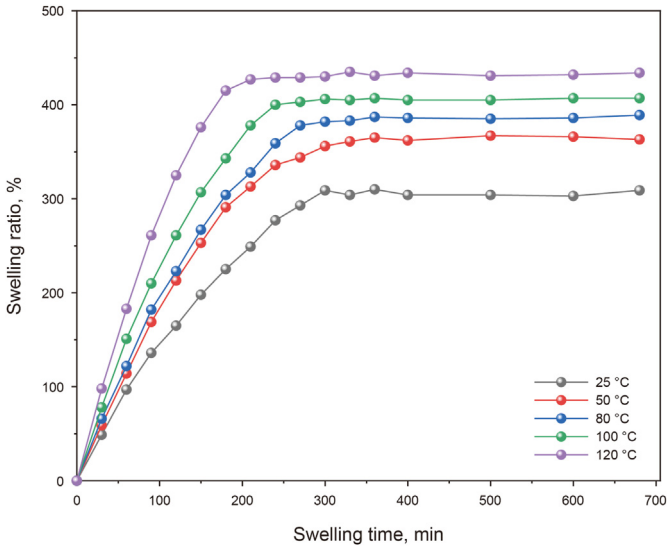

Fig. 9. Swelling kinetics behavior of d_PPGs at different temperatures (50,000 ppm NaCl solution).

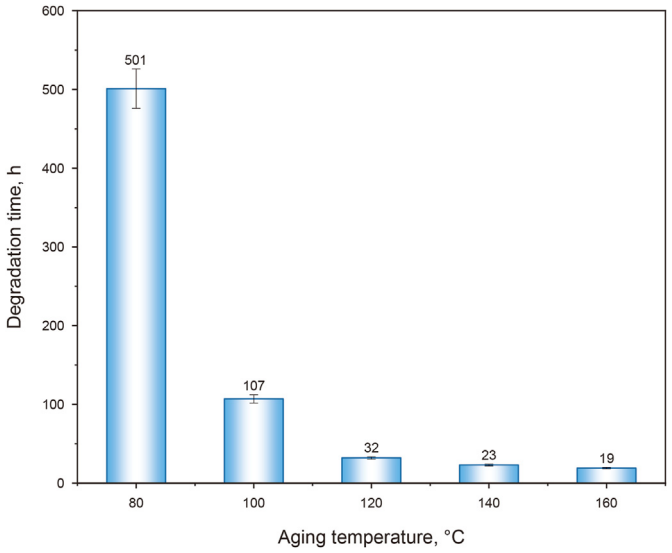

Fig. 10. Self-degradation time of d_PPGs at different temperatures (50,000 ppm NaCl solution).

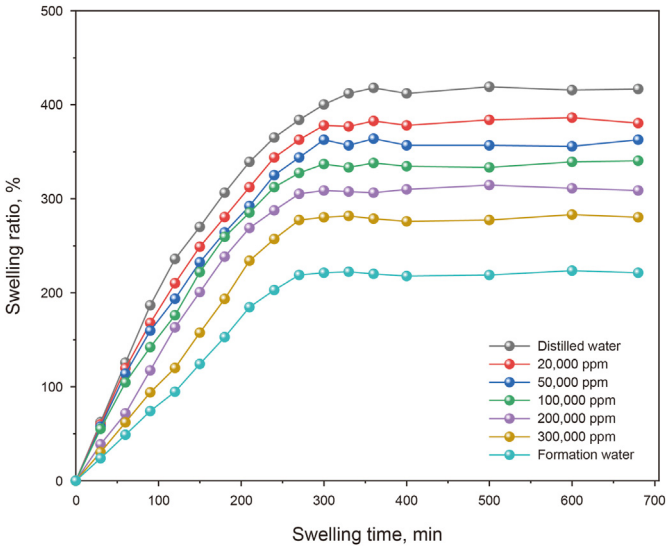

Fig. 12. Swelling kinetics behavior of d_PPGs at different salinities (50 °C).

time higher temperature also accelerates the hydrolysis of the amide groups in the polymer, thus leading to a faster collapse of the d_PPGs structure. The degraded d_PPGs completely converted into liquid without any solid residue (Fig. 11 (a-d)), the viscosity of the degradation solution is less than 5 mPa·s (Fig. 11 (e)). The self-degradability of d_PPGs can be contributed to the instability of the crosslinking structure. The physical crosslinking between Fe^{3+} and COO^{-} is easily damaged by heat, and MBA is also a thermally unstable chemical crosslinking agent, so PPG will degrade at formation temperature due to the damage of the crosslinking structure. This proves that the d_PPGs could be used as a "temporary plugging" measure, which can degrade by itself after the necessary plugging action and will not cause long-term damage to the permeability of the formation.

3.5.2. Effect of salinity on gel swelling kinetics behavior and self-degradation time

Fig. 12 shows the swelling ratio of d_PPGs in different concentrations NaCl solutions (20,000, 50,000, 100,000, 200,000, and 300,000 ppm) with distilled water (DW) and formation water (FW), for comparison. The formation water is the simulated formation water of Tahe Oilfield in China, and its total dissolved salinity (TDS) and ion composition are shown in Table 1. The swelling ratio of

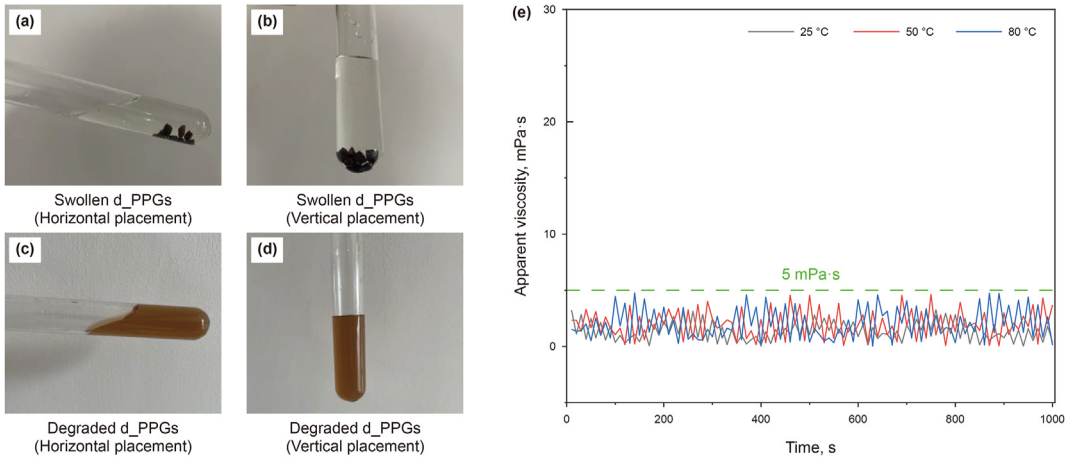

Fig. 11. (**a**–**d**) Morphological changes of d_PPGs before and after degradation. **(e)** The viscosity of the degradation solution.

Table 1
Ion composition of simulated formation water for experiment.

Na^+, mg/L	K^+, mg/L	Ca^{2+}, mg/L	Mg^{2+}, mg/L	Cl^-, mg/L	SO_4^{2-}, mg/L	HCO_3^-, mg/L	TDS, mg/L
78,773.0	419.6	13,721.1	366.5	147,056.2	67.6	72.6	240,476.6

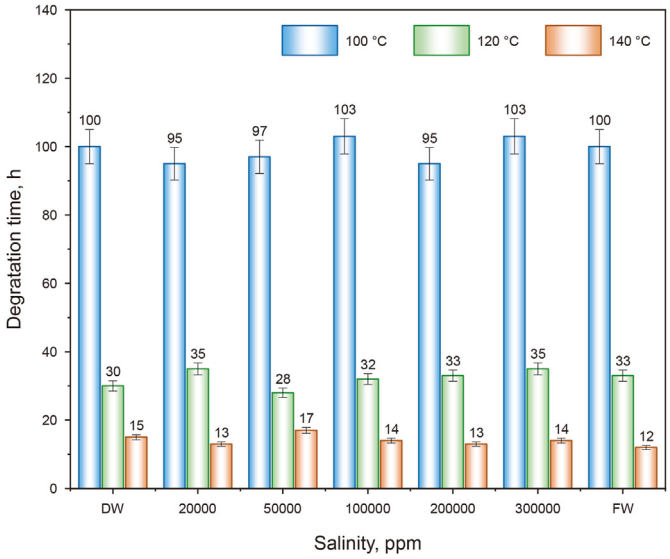

Fig. 13. Self-degradation time of d_PPGs in different salinities and different temperatures.

d_PPGs at different salinities increases rapidly within 350 min and then reaches the ESR. In addition, it could be found that with the increase of salinity, the ESR of d_PPGs gradually decreases, among which, d_PPGs in distilled water has the highest ESR of about 420%, followed by 20,000 ppm NaCl solution, the ESR is about 385%. The increasing salinity caused a decrease in the electrostatic repulsion between anionic segments on the d_PPGs molecules and the osmotic pressure inside and outside the gel network, both of which caused a lower ESR. The ESR of the d_PPGs was the lowest in formation water due to the presence of divalent cations chelating with COO^- in the d_PPGs structure which increases the crosslinking density, ultimately leading to a low swelling ratio (Horkay et al., 2001; Sircar et al., 2013).

The samples of the dried d_PPGs and the NaCl solutions of different concentrations (20,000, 50,000, 100,000, 200,000, and 300,000 ppm) were placed in a hydrothermal reaction kettle and then transferred into a vacuum oven at temperature (100 °C, 120 °C, and 140 °C), to study the influence of salinity on the self-degradation time with distilled water (DW) and formation water (FW) as a control (Fig. 13). The salinity had almost no effect on the self-degradation time of d_PPGs at the same aging temperature, compared with the control group. This behavior is contributed to the presence of the natural polymer sodium alginate in d_PPGs, which is insensitive to cations in the formation, thus resulting in an excellent salt resistance.

3.6. Laboratory coreflooding test

To evaluate the plugging effect on formation fractures, a fracture with a height of 0.8 mm is imitated by a copper sheet with a thickness of 0.8 mm sandwiched in the split core, and it is successfully filled with 16–20 mesh (1.18 mm–0.85 mm) swollen d_PPGs, as shown in Fig. 14 (a-d) (Song et al., 2018). Fig. 14 (e) shows the function of injection pressure and injection time during displacement with key values displayed in Table 2. During the first water flooding, the high permeability caused by the existence of the fracture caused the pressure curve to be flat because there was little resistance towards the flowing water. The injection of 0.5 wt% d_PPGs carried by the guar gum solution caused the injection pressure to rise rapidly and to reach maximum pressure. Thereafter, the injection pressure began to drop, finally stabilizing at 3.70 MPa when the d_PPGs solution flowed through the outlet. Then, the formation water was injected again, increasing the injection pressure to the breakthrough pressure at a maximum of 7.37 MPa. The injection of formation water was continued subsequently, showing

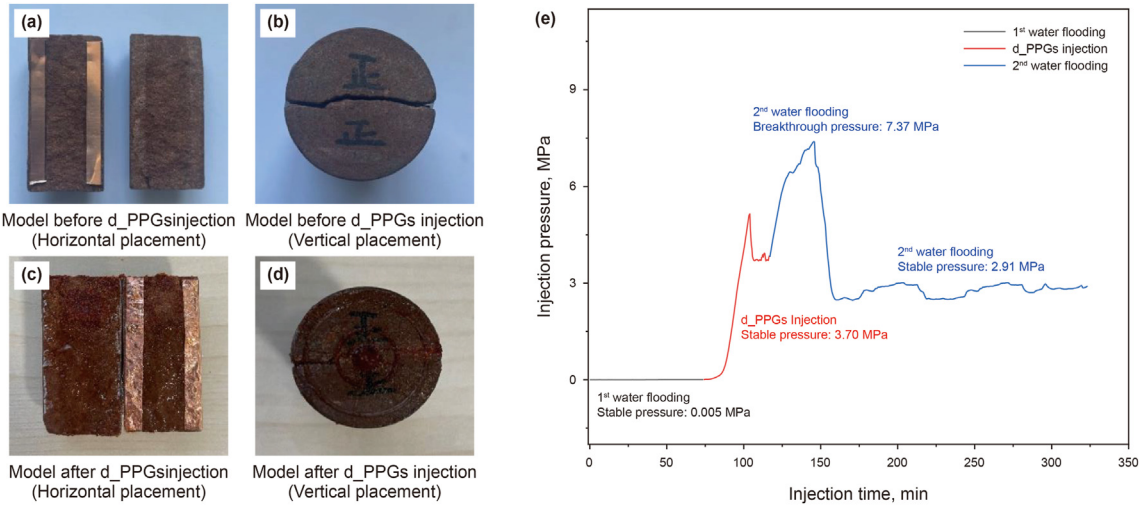

Fig. 14. (**a**–**d**) Core morphology changes before and after plugging. **(e)** Injection pressure changes with time during displacement.

Table 2
Displacement test results.

Core state	Pressure drop, MPa	Flow rate, mL/min	Permeability, 10^{-3} μm^2	Plugging efficiency, %
Before injecting d_PPGs	0.005	0.492	170.444	99.83
After injecting d_PPGs	2.910	0.494	0.286	

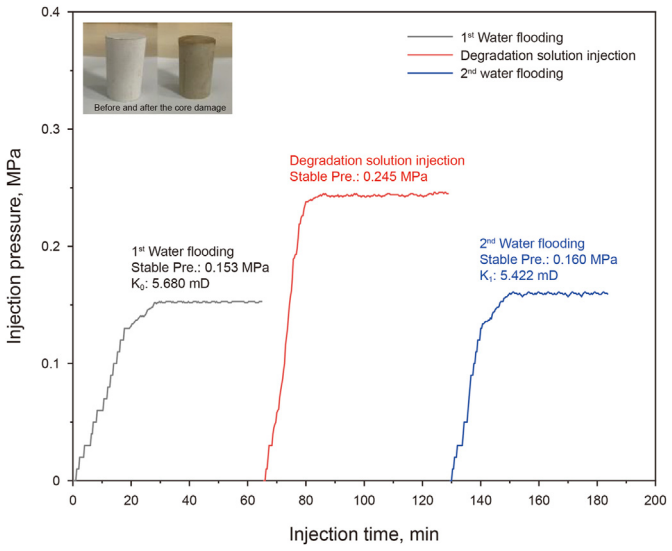

Fig. 15. Damage of degradation solution of d_PPGs to core permeability.

a decrease in the injection pressure, which stabilized at about 2.91 MPa. This shows that the d_PPGs had a high plugging efficiency of 99.83% owing to the high strength of its dual cross-linked structure.

3.7. Core damage experiment

The damage caused by the degraded liquid to the permeability of the formation matrix was tested (Fig. 15), as the formation temperature and sufficient time have been shown to completely degrade the d_PPGs (Fig. 11 (a-d)). The damage ratio of the degradation solution of d_PPGs to the formation matrix was only 4.5%, suggesting that this material would not cause big damage to the reservoir permeability after degradation.

4. Conclusion

To plug fractures/void space conduits in oil and gas formations, and improve the water injection profile, we designed and synthesized a novel type of PPGs with a dual cross-linked structure using SA and AAm. The structure of prepared d_PPGs was firstly characterized by composition and morphology analysis. Then, swelling kinetics behavior, and gel strength and stability of d_PPGs were studied. To evaluate the plugging effect and core damage of d_PPGs, coreflooding test and core damage experiment were performed. The following conclusions were drawn:

(1) We developed a facile method to synthesize d_PPGs using low cost and environment-friendly materials. By the free radical polymerization, d_PPGs possessed a honeycomb-like grid structure, as shown by SEM and FTIR.

(2) The ESR of d_PPGs is lower than that of most conventional PPGs, thus enhancing their potential to migrate deeper into the formation. The ESR and swelling rate increase with increasing temperature and decreasing salinity. Temperature has considerable effect on the self-degradability of d_PPGs, whereas salinity of brines has negligible effect.

(3) The introduction of dual cross-linked structure endows d_PPGs with a better elastic modulus up to 86,445 Pa, to avoid damaging by shearing force when passing through the fractures in formations, thus improving plugging strength.

(4) The laboratory coreflooding test shows that d_PPGs have a very high breakthrough pressure and plugging efficiency. The d_PPGs can be completely degraded under the formation conditions with a degraded liquid viscosity below 5 mPa·s, implying that it would not cause permanent damage to the formation.

Acknowledgements

This work was supported by Shanxi Provincial Key Research and Development Project (No. 20201102002), the Science Foundation of China University of Petroleum, Beijing (No. 2462020BJRC007, 2462020YXZZ003), and State Key Laboratory of Petroleum Resources and Prospecting, China University of Petroleum (No. PRP/DX-2216).

References

Al-Muntasheri, G.A., Nasr-El-Din, H.A., Hussein, I.A., 2007. A rheological investigation of a high temperature organic gel used for water shut-off treatments. J. Petrol. Sci. Eng. 59 (1–2), 73–83. https://doi.org/10.1016/j.petrol.2007.02.010.

Alfarge, D.K., Wei, M.Z., Bai, B.J., 2017. Numerical simulation study of factors affecting relative permeability modification for water-shutoff treatments. Fuel 207, 226–239. https://doi.org/10.1016/j.fuel.2017.06.041.

Amaral, C.N.R., Oliveira, P.F., Roman, I.O., et al., 2019. Preformed particle gels with potential applicability for conformance control of oil reservoirs. J. Appl. Polym. Sci. 137 (15), 48554. https://doi.org/10.1002/app.48554.

Bai, B.J., Liu, Y.Z., Coste, J., et al., 2007. Preformed particle gel for conformance control: transport mechanism through porous media. SPE Reservoir Eval. Eng. 10 (2), 176–184. https://doi.org/10.2118/89468-PA.

Baloochestanzadeh, S., Hassanajili, S., Escrochi, M., 2021. Rheological properties and swelling behavior of nanocomposite preformed particle gels based on starch-graft-polyacrylamide loaded with nanosilica. Rheol. Acta. 60 (10), 571–585. https://doi.org/10.1007/s00397-021-01287-z.

Bao, X.Y., Yu, L., Simon, G.P., et al., 2018. Rheokinetics of graft copolymerization of acrylamide in concentrated starch and rheological behaviors and microstructures of reaction products. Carbohydr. Polym. 192, 1–9. https://doi.org/10.1016/j.carbpol.2018.03.040.

Baumberger, T., Ronsin, O., 2010. Cooperative effect of stress and ion displacement on the dynamics of cross-link unzipping and rupture of alginate gels. Biomacromolecules 11 (6), 1571–1578. https://doi.org/10.1021/bm1002015.

Chen, X., Zhao, L.Q., Liu, P.L., et al., 2021. Laboratory study and field verification of a thermo-responsive water shutoff agent. J. Petrol. Sci. Eng. 201, 108499. https://doi.org/10.1016/j.petrol.2021.108499.

Elsharafi, M.O., Bai, B.J., 2016. Influence of strong preformed particle gels on low permeable formations in mature reservoirs. Petrol. Sci. 13 (1), 77–90. https://doi.org/10.1007/s12182-015-0072-3.

Elsharafi, M.O., Bai, B.J., 2012. Effect of weak preformed particle gel on unswept oil zones/areas during conformance control treatments. Ind. Eng. Chem. Res. 51 (35), 11547–11554. https://doi.org/10.1021/ie3007227.

Fatemi, S.M., Kharrat, R., 2011. Assessment of Vapor Extraction (VAPEX) process performance in naturally fractured reservoirs. J. Petrol. Sci. Eng. 75 (3–4), 260–273. https://doi.org/10.1016/j.petrol.2010.11.018.

Ganguly, S., Willhite, G.P., Green, D.W., et al., 2001. The effect of fluid leakoff on gel placement and gel stability in fractures. SPE J. 7 (3), 309–315. https://doi.org/10.2118/79402-PA.

Horkay, F., Tasaki, I., Basser, P.J., 2001. Effect of monovalent– divalent cation exchange on the swelling of polyacrylate hydrogels in physiological salt solutions. Biomacromolecules 2 (1), 195–199. https://doi.org/10.1021/bm0056153.

Imqam, A., Bai, B.J., 2015. Optimizing the strength and size of preformed particle gels for better conformance control treatment. Fuel 148, 178–185. https://doi.org/10.1016/j.fuel.2015.01.022.

Kang, W.L., Hu, L.L., Zhang, X.F., et al., 2015. Preparation and performance of fluorescent polyacrylamide microspheres as a profile control and tracer agent. Petrol. Sci. 12 (3), 483–491. https://doi.org/10.1007/s12182-015-0042-9.

Khoshkar, P.A., Fatemi, M., Ghazanfari, M.H., 2020. Static and dynamic evaluation of the effect of nanomaterials on the performance of a novel synthesized PPG for water shut-off and improved oil recovery in fractured reservoirs. J. Petrol. Sci. Eng. 189 (2), 107019. https://doi.org/10.1016/j.petrol.2020.107019.

Li, J., Illeperuma, W., Suo, Z., et al., 2014. Hybrid hydrogels with extremely high stiffness and toughness. ACS Macro Lett. 3 (6), 520–523. https://doi.org/10.1021/mz5002355.

Li, X., Song, X., Yue, X.A., et al., 2007. Effects of shear fracture on in-depth profile modification of weak gels. Petrol. Sci. 4 (1), 55–60. https://doi.org/10.1007/BF03186574.

Li, Y., Li, Y., Yang, P., 2019. Water shutoff and profile control in China over 60 years. Oil Drilling & Production Technology 41, 773–787. https://doi.org/10.13639/j.odpt.2019.06.016.

Lin, P., Ma, S.H., Wang, X.L., et al., 2015. Molecularly engineered dual-crosslinked hydrogel with ultrahigh mechanical strength, toughness, and good self-recovery. Adv. Mater. 27 (12), 2054–2059. https://doi.org/10.1002/adma.201405022.

Liu, X.Y., Xu, H., Zhang, L.Q., et al., 2019. Homogeneous and real super tough multibond network hydrogels created through a controllable metal ion permeation strategy. ACS Appl. Mater. Interfaces 11 (45), 42856–42864. https://doi.org/10.1021/acsami.9b18620.

Liu, Y.Z., Bai, B.J., Wang, Y.F., 2010. Applied technologies and prospects of conformance control treatments in China. Oil Gas Sci Technol–Revue d'IFP Energy Nouvelles. 65 (6), 859–878. https://doi.org/10.2516/ogst/2009057.

Liu, Z.L., Zhao, G., Brewer, M., et al., 2021. Comprehensive review on surfactant adsorption on mineral surfaces in chemical enhanced oil recovery. Adv. Colloid Interface Sci. 294, 102467. https://doi.org/10.1016/j.cis.2021.102467.

Masulli, M., Liu, Z.L., Guo, F.Z., et al., 2021. Temperature effect on the dynamic adsorption of anionic surfactants and alkalis to silica surfaces. Petrol. Sci. https://doi.org/10.1016/j.petsci.2021.11.008. In press.

Patel, M.A., Aboughaly, M.H., Schryer-Praga, J.V., et al., 2017. The effect of ionotropic gelation residence time on alginate cross-linking and properties. Carbohydr. Polym. 155, 362–371. https://doi.org/10.1016/j.carbpol.2016.08.095.

Pu, J.Y., Gu, X.Y., Luo, M.L., et al., 2021. Polyelectrolyte complex induced Stimuli-responsive Self-association and reinforcement of interpenetrated Poly(acrylamide-co-vinyl acetate)/alginate particles for fossil energy recovery. J. Mol. Liq. 343, 117596. https://doi.org/10.1016/j.molliq.2021.117596.

Qiu, Y., Wei, M.Z., Bai, B.J., 2017. Descriptive statistical analysis for the PPG field applications in China: screening guidelines, design considerations, and performances. J. Petrol. Sci. Eng. 153, 1–11. https://doi.org/10.1016/j.petrol.2017.03.030.

Salunkhe, B., Schuman, T., Al Brahim, A., et al., 2021. Ultra-high temperature resistant preformed particle gels for enhanced oil recovery. Chem. Eng. J. 426, 130712. https://doi.org/10.1016/j.cej.2021.130712.

Seright, R., Brattekas, B., 2021. Water shutoff and conformance improvement: an introduction. Petrol. Sci. 18 (2), 450–478. https://doi.org/10.1007/s12182-021-00546-1.

Singh, R., Mahto, V., 2017. Synthesis, characterization and evaluation of polyacrylamide graft starch/clay nanocomposite hydrogel system for enhanced oil recovery. Petrol. Sci. 14 (4), 765–779. https://doi.org/10.1007/s12182-017-0185-y.

Sircar, S., Keener, J.P., Fogelson, A.L., 2013. The effect of divalent vs. monovalent ions on the swelling of Mucin-like polyelectrolyte gels: governing equations and equilibrium analysis. J. Chem. Phys. 138 (1), 014901. https://doi.org/10.1063/1.4772405.

Song, L.F., Ge, J.J., Wu, H., et al., 2019. Preparation and performance evaluation of crosslinked polymer particle with temperature resistance and salt tolerance. Oilfield Chem. 36 (3), 415–421. https://doi.org/10.19346/j.cnki.1000-4092.2019.03.007.

Song, Z.J., Bai, B.J., Zhang, H., 2018. Preformed particle gel propagation and dehydration through semi-transparent fractures and their effect on water flow. J. Petrol. Sci. Eng. 167, 549–558. https://doi.org/10.1016/j.petrol.2018.04.044.

Sun, J.Y., Zhao, X., Illeperuma, W.R., et al., 2012. Highly stretchable and tough hydrogels. Nature 489 (7414), 133–136. https://doi.org/10.1038/nature11409.

Sun, X.D., Bai, B.J., 2017. Comprehensive review of water shutoff methods for horizontal wells. Petrol. Explor. Dev. 44 (6), 1022–1029 (**in Chinese**).

Tongwa, P., Bai, B.J., 2014. Degradable nanocomposite preformed particle gel for chemical enhanced oil recovery applications. J. Petrol. Sci. Eng. 124, 35–45. https://doi.org/10.1016/j.petrol.2014.10.011.

Touzé, S., Guerin, V., Guezennec, A.G., et al., 2015. Dissemination of acrylamide monomer from polyacrylamide-based flocculant use—sand and gravel quarry case study. Environ. Sci. Pollut. Res. 22 (9), 6423–6430. https://doi.org/10.1007/s11356-014-3177-0.

Wu, Q.H., Ge, J.J., Zhang, G.C., et al., 2019. The water shutoff simulation experiment using tube for high-strength plugging agent in fractured reservoir. Acta Pet. Sin. 40 (11), 1368. https://doi.org/10.7623/syxb201911007.

Yang, C.H., Wang, M.X., Haider, H., et al., 2013. Strengthening alginate/polyacrylamide hydrogels using various multivalent cations. ACS Appl. Mater. Interfaces 5 (21), 10418–10422. https://doi.org/10.1021/am403966x.

Ye, L., Tang, Y.J., Qiu, D., 2014. Enhance the mechanical performance of polyacrylamide hydrogel by aluminium-modified colloidal silica. Colloids Surf. A Physicochem. Eng. Asp. 447, 103–110. https://doi.org/10.1016/j.colsurfa.2014.01.072.

Zhao, G., Dai, C.L., Chen, A., et al., 2015. Experimental study and application of gels formed by nonionic polyacrylamide and phenolic resin for in-depth profile control. J. Petrol. Sci. Eng. 135, 552–560. https://doi.org/10.1016/j.petrol.2015.10.020.

Zhao, L.Q., Chen, X., Zou, H.L., et al., 2020. A review of diverting agents for reservoir stimulation. J. Petrol. Sci. Eng. 187, 106734. https://doi.org/10.1016/j.petrol.2019.106734.

Zheng, H.C., Yang, J.S., Han, S.Y., 2016. The synthesis and characteristics of sodium alginate/graphene oxide composite films crosslinked with multivalent cations. J. Appl. Polym. Sci. 133 (27), 43616. https://doi.org/10.1002/app.43616.

Zhou, Q., Kang, H., Bielec, M., et al., 2018. Influence of different divalent ions crosslinking sodium alginate-polyacrylamide hydrogels on antibacterial properties and wound healing. Carbohydr. Polym. 197, 292–304. https://doi.org/10.1016/j.carbpol.2018.05.078.

Zhu, D.Y., Bai, B.J., Hou, J.R., 2017. Polymer gel systems for water management in high-temperature petroleum reservoirs: a chemical review. Energy Fuel. 31 (12), 13063–13087. https://doi.org/10.1021/acs.energyfuels.7b02897.

Zhu, D.Y., Fang, X.Y., Sun, R.X., et al., 2020. Development of degradable pre-formed particle gel (DPPG) as temporary plugging agent for petroleum drilling and production. Petrol. Sci. 18 (2), 479–494. https://doi.org/10.1007/s12182-020-00535-w.